Low power plasma spray assisted thermal barrier coating repair without the plugging of cooling holes

Frédéric Rousseau, Cédric Guyon, Daniel Morvan, Marie-Pierre Bacos, Odile Lavigne, Catherine Rio, C. Guinard, Baptiste Chevillard

Low power plasma spray assisted thermal barrier coating repair without the plugging of cooling holes

F. ROUSSEAU[a], C. GUYON[a], D. MORVAN[a]

[a] Chimie ParisTech, PSL Research University, CNRS, Institut de Recherche de Chimie Paris (IRCP), F-75005 Paris, France

M.- P. BACOS[b], O. LAVIGNE[b], C. RIO[b]

[b] ONERA, DMAS, Université Paris-Saclay, F-92322 Châtillon, France

C. GUINARD[c]

[c] Centre de Réparation et de Maintenance Aéronautique, Air France Industrie, Elancourt, France

B. CHEVILLARD[d]

[d] Ateliers Industriels Aéronautiques de Bordeaux, Ministère de la Défense, France

*Corresponding author: Dr Frederic ROUSSEAU

Phone number: +33185784254

Email: frederic.rousseau@chimieparistech.psl.eu

Abstract

Currently operating new generation aircraft engines are equipped with multi-hole combustion chambers, coated with a thick ZrO_2-4 mol% Y_2O_3 (YpSZ) Thermal Barrier Coating (TBC). The local repair of such multi-hole combustors requires the development of specific deposition methods. This paper describes a modified version of a Low Power Plasma Reactor (LPPR), upgraded with two opposite gas flows to prevent cooling channel plugging. The influence of some experimental parameters (plasma power density, spray distance and precursor concentration) on the repaired TBC microstructure is examined. A short spray distance, associated with a low power density and a low concentration of nitrate precursors, led to a suitable microstructure of the deposited YpSZ. Moreover, FTIR spectroscopy and SEM-EDS analysis revealed the efficient conversion of the nitrate precursors into oxide and the good infiltration of the deposited YpSZ into the damaged area. Finally, it is shown that, once the deposition parameters have been optimized, a dual flow system effectively allows local repair to be carried out without plugging the cooling system.

Keywords

LPPR, damaged TBC, local repair, liquid precursors, infiltration, dual flow.

1. Introduction

Thermal Barrier Coating (TBC) systems are used in aircraft gas turbines to prevent high-temperature degradation of metallic structures in the combustor and high-pressure turbine parts **[1-2]**. TBC consists of a porous ceramic oxide layer (typically Yttria partially Stabilized Zirconia –YpSZ) deposited onto an alumina-forming metallic bond coat (BC), which ensures the protection from oxidation of the underlying nickel-based alloy **[3-5]**.

Currently operating new generation aircraft engines are equipped with multi-hole combustion chambers. The channels are fed with cooling air drawn from the compressor and heat exchange takes place by forced convection through the holes and by conduction through the chamber material itself. The cool air feed to the holes produces a protective film on the inner face of the wall, downstream from the flow, between the wall and the burnt gases created by combustion in the chamber. Given that the durability of the TBC is limited due to several damage or erosion mechanisms **[1, 6]**, the combustion chamber must be changed or repaired. Repair methods can partially obstruct the cooling system and reduce its cooling efficiency. As a consequence, higher temperature distributions can occur and promote thermally induced stresses, undesired

oxidation of the chamber material, TBC failure, etc., which degrade the combustor efficiency, integrity and lifetime.

Many solutions have been proposed to prevent the obstruction of the cooling system during the repair. Some patents claim methods using stoppers that can evaporate afterwards, or masks that are placed individually in each hole **[7]**, or in several holes at a time **[8, 9]**. However, all of these methods are expensive, both in time and tooling. Other ways consist in injecting water at a very high pressure **[10]** into the permeable component, with or without an aggressive product such as sodium hydroxide **[11]**, or an abrasive solution **[12]**. Nevertheless, these methods can lead to the erosion of the cooling channels, to the formation of oxides or to the presence of unexpected corrosive compounds inside them. As a result, the most common practice is to remove the entire bond coat as well as the TBC before depositing new coatings on the whole chamber, and to drill all of the cooling holes again **[13]**. In most cases, only local damages of the TBC are identified and a local repair method should be less expensive.

Recent work on a laboratory scale proved that YpSZ locally deposited by a Low Power Plasma Reactor (LPPR) heals the damage and welds internal delamination cracks **[14, 15]**. In order to be implemented as an industrial process, this repair technique must also prevent the plugging of the cooling system during the local deposition. This paper describes a new prototype of the

Low Power Plasma Reactor to locally repair the thermal barrier coating of portions of a multi-hole combustion chamber without clogging the cooling system. This equipment operates with two gas flows: one transports the precursors into the plasma allowing the deposition of YpSZ; the second gas circulates through the cooling channels and prevents their clogging.

Firstly, the influence of reactor parameters such as power density, spray distance and precursor concentration on the YpSZ coating composition / microstructure was studied. The objective was to determine the value of these parameters that would allow the deposition of a YpSZ coating with a homogeneous and stable microstructure compatible with that of a conventional Air Plasma Spray TBC. Secondly, repair experiments following optimized deposition parameters and using the two-gas stream were conducted to locally repair damaged TBC on combustor parts.

2. Materials and methods

2.1 Scaled-up low power plasma reactor

A laboratory-scale Low Power Plasma Reactor (LPPR) was initially developed to deposit porous oxide layers for protecting combustor walls **[15-17]**. The LPPR is based on spraying an aqueous solution of inexpensive and non-toxic liquid nitrate precursors $ZrO(NO_3)_2$ and $Y(NO_3)_3$ into a low-pressure plasma. Given that this plasma contains species such as O and

OH°, it is used as an oxidant medium at moderate temperature, which is able to transform the nitrates into a deposited solid oxide layer of ZrO_2-4 mol% Y_2O_3 (called YpSZ throughout this paper) **[18]**. The first laboratory reactor only allowed flat surfaces up to 25 mm × 25 mm = 625 mm^2 to be coated **[15]**. Therefore, a scaled-up LPPR device was developed to deposit YpSZ onto larger surfaces, which should be more representative of parts of a combustion chamber typically 50 mm × 50 mm = 2500 mm^2. Furthermore, it was equipped to prevent the cooling holes from being closed during YpSZ deposition.

A diagram of this scaled-up LPPR is given in Fig. 1. It consists of a quartz tube (100 mm internal diameter, 600 mm length) coupled with two microwave generators (2.5 GHz – SAIREM GMP 20KE/D) for the plasma discharge (power range 1-4 kW). Argon and oxygen gases are introduced into the reactor using Bronkhorst F 201-C flow meters (0 to 5000 mL min^{-1} each under Standard Temperature and Pressure conditions). A vacuum pump (Pfeiffer 2063C2) allows the pressure in the reactor to be decreased (700-1200 Pa). The pressure is measured in real time with a Pirani type gauge (Pfeiffer PPT200). The detailed description of the liquid injection system was reported in a previous paper **[15]**. It is equipped with a mixing chamber containing two capillaries (0.53 mm in diameter). The first one allows the liquid precursor solution to be aspired while the second one draws the argon gas. A pulsed solenoid

valve is used to control the flow of the liquid gas mixture, which is transferred to a nozzle through a stainless-steel tube (6.35 mm in diameter). The valve opening and closing time ranges were, respectively, t_{on}: 0.1-1 s and t_{off}: 1-10 s. The 0.7-mm diameter nozzle (manufactured by Spraying Systems Co.) enables small droplets to be produced by dual-flow atomization. This injector thereby produces a homogeneous and reproducible spray, as reported in previous works **[15]**. The spray has an angle of dispersion of 13.5° and all the velocity and diameter values for droplets have been already published in a previous paper **[15]**. In the laboratory-scale LPPR, the nozzle-substrate distance and the plasma power were fixed and respectively equal to 240 mm and 240 W. It was proved that these experimental parameters allowed the precursors to be deposited onto the substrate in liquid form producing a successful infiltration and repair of the damaged TBC **[15]**.

In the scaled-up LPPR it is possible to adjust the plasma power from 1200 to 3000 W and the distance between the atomization nozzle and the surface to be coated - called the spray distance (d_{spray}) - from 240 to 500 mm. These new parameters provide additional degrees of freedom compared to the lab-scale reactor. The spray distance can have a great influence on the microstructure of the deposited layers in terms of homogeneity, pore size, etc. However, increasing the spray distance significantly can lead to a drastic decrease in the amount deposited

per unit area, as illustrated in Fig. 1 (right). Indeed, with the maximal spray distance of 500 mm the diffused spray is larger than the part to be coated, leading to high raw material (nitrate precursors) waste. This point is discussed later in Section 3, for example, when growth rates of several samples are compared as a function of d_{spray}.

Whatever the spray distance, the substrate holder remains always in the plasma discharge. Given that the substrate holder is almost as large (6650 mm^2) as the reactor passage section (7854 mm^2), the discharge between the substrate and the reactor inlet is confined. As shown in Figure 1, the nozzle is located 20 mm below the reactor inlet. The power density of the plasma discharge δ_p (W mm^{-3}) can be estimated as follows:

$$\delta_p = Pw / V_d \qquad \text{Eq. (1)}$$

where:

Pw: plasma power (W)

V_d: volume available for the discharge (mm^3) = $(d_{spray} + 20) \times S_{reactor}$ Eq. (2)

d_{spray}: spray distance (mm) and $S_{reactor}$: reactor section = $\pi \times (50)^2$ = 7854 mm^2.

In order to repair multi-hole combustor parts, an additional gas flow can be injected through the substrate holder **[19]**. The principle consists in connecting the part to be repaired to the substrate holder with a tight seal made of silicon (CAF4). Then, the protective gas is injected through both the rear face of the substrate holder and the part to be repaired. Thus, two opposite gas flows should be managed during the repair (see Section 2.3): one transporting the nitrate precursors into the plasma and enabling YpSZ deposition, and the second one (a protective gas) circulating through the cooling holes and preventing them from becoming clogged, as shown in Fig. 2.

2.2 Coating and repair experiments

All flows mentioned in this paper are given under STP (Standard Temperature and Pressure) conditions. All the LPPR data explored or fixed for the deposition of YpSZ coatings by LPPR are summarized in Table 1. A mixture of Ar / O_2 is used to produce the oxidizing microwave plasma discharge (Ar: 2000 mL min^{-1} and O_2: 500 mL min^{-1}) when the power is turned on. The nitrate precursors (Aldrich, 99% purity) are dissolved in deionized water at the following concentrations: $[ZrO(NO_3)_2] = 3.4 \times 10^{-1}$ mol L^{-1} and $[Y(NO_3)_3] = 2.96 \times 10^{-2}$ mol.L^{-1} (standard

solution-Std), corresponding to an expected composition of ZrO_2 + 4 mol% Y_2O_3 or 7.4 wt% Y_2O_3. The injection of this standard nitrate solution is carried out according to the argon flow rate and the valve control parameters described hereafter. The mixture of argon gas (2000 mL min^{-1}) and aqueous solution (5 mL min^{-1}) is automatically injected for 1 min through the pulsed valve (opening and closing times t_{on} = 0.8 and t_{off} = 1 s). The pressure in the reactor varies from 1200 to 800 Pa depending on whether the valve is open or closed. After the injection of the liquid (i.e., the valve being closed), the pressure is stabilized at 700 Pa, the Ar / O_2 plasma is maintained in order to transform the deposited nitrates into an oxide coating ("post-treatment" step that typically lasts 9 minutes), and then the discharge is stopped. It is worth noting that, although the temperatures of both the substrate and the reactor remain lower than 400 °C during the post treatment, it is essential to cool for 5 min to preserve the reactor against thermal shock. After the reactor has cooled down, another cycle (injection followed by a post treatment and cooling) can be carried out. These cycles can be repeated as long as necessary to obtain the desired thickness of the deposited oxide. Finally, the oxide coating can be annealed at T=1000 or 1100 °C for 2 h, in order to enhance the crystallization of the oxide and the formation of nano porosities (as previously described **[15-18]**). This annealing is optional and could be performed during the first use in a real turbine engine.

Deposition experiments were performed first on flat substrates (25 mm diameter, 2 mm thickness) of dense alumina to study the influence of plasma power, spray distance and precursor concentration on the deposited YpSZ microstructure. Other deposition tests were performed on Hastelloy X substrates (25 mm diameter, 2 mm thickness), coated with an Air Plasma Spray (APS) NiCrAlY bond coat (100 µm thick), to optimize repair conditions. The bond coat was deposited using NiCrAlY powder : Amdry 962 alloy type (Ni: 67, Cr: 22, Al: 10, Y_2O_3: 1 in wt%). In all cases the samples were annealed at 1100 °C / 2h.

Secondly, local repair experiments were performed on parts (50 mm × 50 mm) cut from a real combustion chamber made of Hastelloy X coated with an APS NiCrAlY bond coat and a YpSZ TBC. Several cooling holes were visible on the surface of the original APS YpSZ. Controlled local spallation zones of different sizes and depths were created artificially in the ceramic coating with a milling micromachine, in order to simulate damaged areas to be repaired. As-coated and repaired samples were analyzed by several techniques. Fourier Transform Infrared Spectroscopy was used to study the chemical bonds present in the coatings (Agilent Spectrometer / 4000-600 cm^{-1}). Sample cross-sections were polished with SiC polishing disks (1200 and 2400 grit) and diamond paste (6, 3 and 0.25 µm). Surface and polished cross-sections were observed with a high-resolution field emission gun scanning electron microscope (FEG-

SEM, ZEISS Gemini DSM982). Energy Dispersive X-ray Spectroscopy (EDS) was used to determine the chemical composition.

2.3 Method for protecting the cooling channels during deposition

The gas flow coming out of the cooling holes prevents the sprayed liquid solution from penetrating inside to form YpSZ. However, it was important to find a good balance in this protective flow because:

- A too high flow rate at the exit of the holes inhibits the formation of the deposit in its surroundings. This results in areas near the holes that may not be covered with YpSZ, leaving the surface without thermal protection.
- Conversely, a too low flow rate does not prevent the solution from penetrating and depositing undesirable YpSZ inside the channels.

To be efficient, the mass flow of the protective gas injected at the sample rear face must be adjusted between the two limits indicated, as described and reported in **[19]**:

- High boundary α: $F_{m\,holes} \leq F_{m\,prec}$ Eq. (3)

where $F_{m\ holes}$ is the mass flow (kg s^{-1}) of the protective fluid through the channels of the permeable substrate and $F_{m\ prec}$ is the mass flow (kg s^{-1}) of the carrier gas loaded with precursors,

- Low boundary β: $F_{m\ holes} \geq F_{m\ prec} \times (\Sigma S_{poro} / S_{reac})$ Eq. (4)

where ΣS_{poro} is the total area (m^2) of the holes in the permeable substrate and S_{reac} (m^2) is the section of the plasma reactor. ΣS_{poro} is calculated considering the number of holes N_{holes} in the area to be repaired (typically 80 for a 50 × 50 mm^2 section of a component) and D is the representative diameter of the multi-hole component (typically 0.5 mm).

Another limiting working condition is linked to the fact that a laminar flow must be maintained (Reynolds number < 2100) at the outlet of the cooling holes to avoid local disruptions and extinguishing of the plasma discharge. The Reynolds number is estimated at the outlet of the holes by the following formula:

$$Re_{holes} = (F_{m\ holes} \times D)/(N_{holes} \times \mu \times \frac{\pi D^2}{4}) \quad \text{Eq . (5)}$$

where μ = dynamic viscosity of the fluid injected (Pa s).

3. Results and discussion

3.1 Relation between the power density of the discharge and the plasma power according to the spray distance

Fig. 3 shows the evolution of the power density δ_p as a function of the power applied to the plasma by the microwave generators for two spray distances (d_{spray}: 240 and 500 mm). In comparison, the estimated average δ_p for the laboratory-scale LPPR previously described was around 6×10^{-4} W mm^{-3} for the deposition of YpSZ (spray distance of 240 mm and plasma power of 240 W) **[15]**. It is worth noting that the maximum power density is equal to 1.47×10^{-3} W mm^{-3} for a power value of 3000 W and a spray distance of 240 mm, in the case of this new LPPR. This power density value of 1.47×10^{-3} W mm^{-3} is 2.5 times higher than that usually reached in the laboratory-scale LPPR. Fig. 3 also reports that, for the same spray distance of 240 mm, the power density δ_p is almost always higher than that of the laboratory-scale reactor, while it is almost always lower for a spray distance of 500 mm. Moreover, it is possible to reach the same power density with two different spray distances by adjusting the plasma power. For example, a power density equal to 7.35×10^{-4} W mm^{-3} is reached for the following spray distance / plasma power parameter: 240 mm / 1500 W and 500 mm / 3000 W.

Several deposition experiments were performed by varying power density and spray distance to determine the influence of these parameters on the microstructure of the deposited LPPR YpSZ.

3.2 Influence of the plasma discharge power density on the deposited LPPR YpSZ composition

Tests were performed with the greatest spray distance (500 mm). Alumina substrates were used to deposit LPPR YpSZ at high ($\delta_p = 7.35 \times 10^{-4}$ W mm^{-3}) and low power density ($\delta_p = 3 \times 10^{-4}$ W mm^{-3}); i.e., for plasma powers of 3000 and 1200 W, respectively. In all cases, the deposition conditions are those described in Section 2.2. The total deposition time was 5 hours (including the cooling step) and the volume of the standard injected solution was 100 mL per experiment. YpSZ deposits were further annealed in a furnace under laboratory air at 1100 °C for 2 h (heating and cooling rate 50 °C.h^{-1}).

FTIR spectroscopy analyses were carried out on the YpSZ layers deposited with both low and high power densities (see Fig. 4). Water, nitrate and oxide bands are observed at around 3400, 1400 and 400 cm^{-1}, respectively. Irrespective of the power density, the oxide band is much more

intense than that of the nitrates in the coating deposited, suggesting that oxidation took place even for the low plasma power density. However, in this case the presence of significant nitrate and water bands also underlines that this condition did not ensure a 100% conversion of nitrates into oxides. After annealing, the FTIR spectrum only showed oxide bands. The addition of thermal energy through the annealing seemed to completely eliminate the nitrates and the residual water.

For high power density (7.35×10^{-4} W.mm^{-3}) and before the annealing step, only traces of water and nitrates can be seen on the FTIR spectrum and the oxide band is then much more intense than the others. This reflects an excellent nitrate to oxide conversion.

All of these results validate the reactivity of the microwave plasma, even with a large spray distance (500 mm). They also reveal that a high power density (i.e., a high plasma power) value is needed to entirely ensure the nitrate to oxide conversion.

3.3 Influence of the power density / plasma power on the deposited LPPR YpSZ microstructure

Experiments were carried out with a great spray distance (500 mm) and different power density values (3×10^{-4}, 4.2×10^{-4} and 7.35×10^{-4} W mm^{-3}) to study the effect on the YpSZ

microstructure. In all experiments, it was observed that a large spray distance of 500 mm led to an important loss of raw material due to deposition on the reactor walls. Fig. 5 shows the microstructure of LPPR YpSZ and demonstrates that the higher the power density, the higher the coating porosity (in terms of hole / shell size) and, consequently, the higher the growth rate.

Previous FTIR analysis revealed (see Section 3.2) that a high power density allows nitrates to be efficiently converted into oxides. However, observations of cross-sections in Fig. 5 demonstrated that a high plasma power associated with a long spray distance lead to the formation of hollow spheres, which affects the microstructure and the strength of the coating.

Surface views of these shells formed at high density power and visible in the cross-section of the LPPR YpSZ are shown in Fig. 6. These hollow spheres are of various sizes, from a few microns to several tens of microns, and of various morphologies: they can have a solid and smooth surface, or a lace-shaped microstructure. These shells should provide low mechanical strength and a poor adherence of LPPR YpSZ coatings on the substrate.

From the observations in Fig. 5, it was assumed that a low plasma power density significantly limited shell formation and led to denser coatings, as if the precursors crushed like splats on

impacting the substrate. Indeed, it can also be pointed out that the lower the plasma density, the lower the deposition rate. The denser microstructure of LPPR YpSZ without shells should be related to the liquid state of the nitrates when impacting the substrate, given that the dehydration time of the nitrated precursors depends on the plasma density value **[20]**. However, simply reducing the power of the plasma and therefore the power density, without modifying this long spray distance, may not be an appropriate solution: an annealing step would have to be added to ensure the total conversion of nitrates into oxides, and there would be losses of material on the reactor walls at each deposition.

The dehydration time also depends on the spray distance. A short distance could limit the evaporation of nitrates so that they impact the substrate in a liquid state. A good adjustment of these two parameters (power density and spray distance) should allow an efficient conversion of nitrates to be associated with a shell-free microstructure for LPPR YpSZ.

3.4 Influence of the spray distance on the deposited LPPR YpSZ microstructure

Fig. 7 shows cross-section SEM micrographs of LPPR YpSZ deposited with the same high power density (δ_p equal to 7.35×10^{-4} W mm^{-3}), but by considering two different spray distances

(240 and 500 mm). As expected, the loss of raw material on the reactor walls was lower when the projection distance was decreased to 240 mm.

Although the growth rates were found to be equal to 20 µm. h^{-1} for both samples, the microstructures of the deposited LPPR layers are totally different due to the variation in the spray distance. It is worth noting that YpSZ coatings deposited with a large spray distance (500 mm) are highly porous and present lots of hollow spheres (shells), as previously described in Section 3.3.

At a short spray distance of 240 mm, the corresponding denser YpSZ coating has a smooth surface and adheres well to the substrate. The pores were on average about 10 microns in width and were quite equally distributed throughout its depth. In this case, the observed faces of the porosity are not representative of the presence of hollow spheres. A densification of the YpSZ is observed toward the substrate, suggesting a process of compaction / crushing of the material and infiltration of nitrates into the opening porosities formed by degassing.

The shells observed in the coatings deposited with a long spray distance probably originate from the precipitation of the nitrate precursors during the flight time. Actually, the combination of a vacuum (700 Pa) and a high plasma power quickly dehydrates the solution as described

previously **[20]**. Furthermore, during a long transit time (long spray distance) of the droplets before they impact the substrate, precipitation can occur in flight and thus promote the formation of hollow spheres.

As a consequence, a reduced spray distance coupled with a moderate plasma power (for example 7.35×10^{-4} W mm^{-3} / 240 mm and 1500 W) seems perfectly suitable for obtaining better quality YpSZ layers such as those shown in Fig. 7 (bottom). This set of parameters promotes the impact of the material, the crushing, the conversion of nitrates and homogenizes the porous / segmented / lamellar morphology of the LPPR YpSZ. An almost 100 % conversion of nitrates into YpSZ before annealing was validated by FTIR (not shown here) as expected, with the high power density of 7.35×10^{-4} W mm^{-3}. With these experimental parameters, the annealing at high temperature is not necessary any more to obtain YpSZ 100% converted from nitrates.

3.5 Influence of the precursor solution concentration on the LPPR YpSZ coating microstructure

To evaluate the impact of the dehydration step of the precursors on the TBC microstructure, other experiments were carried out on APS MCrAlY coated superalloy substrate. These experiments were performed on the basis of the parameters described in Section 2.2 and considering the results of Section 3.4: a plasma power of 1500 W ($\delta p = 7.35 \times 10^{-4}$ W mm^{-3}) and a spray distance of 240 mm. Nitrate solutions with two different dilutions were tested: the standard one (Std) and a diluted solution (Std$^{1/2}$) corresponding to 1 volume of standard solution diluted in 1 volume of distilled water. The deposition was conducted in three steps, successively injecting 200 mL of the Std$^{1/2}$ solution, then 200 mL of the Std solution and, finally, 100 mL of the Std$^{1/2}$ solution again. The resulting coating microstructure is shown in Fig. 8.

It appears that the YpSZ layers obtained with the diluted solution (Std$^{1/2}$) are denser, but thinner than that deposited with the standard solution (Std). Using the (Std$^{1/2}$) solution instead of the standard one, the growth rate is reduced to 10 µm / h (instead of 20 µm / h) and the yield is equal to 0.25 µm / mL of nitrate solution (instead of 0.4 µm / mL).

Further YpSZ deposition experiments were performed on an APS MCrAlY bond coat and alumina substrate using the diluted solution (Std$^{1/2}$) only. A 100-µm-thick YpSZ coating was obtained from 400 mL of (Std$^{1/2}$) solution after 10 h of deposition on a MCrAlY bond coat (Fig. 9). Whatever the substrate, the growth rate was about 10 µm / h and the yield was estimated at

0.25 µm / mL of nitrate solution. The obtained microstructure of the LPPR YpSZ coating is in agreement with that shown in Fig. 8, corresponding to the diluted solution; i.e., presence of rounded pores not exceeding 20 µm in diameter and vertical cracks. SEM-EDS analysis confirms the homogeneity of the composition throughout the coating as ZrO_2-4 mol% Y_2O_3. XRD analyses (not included herein) showed that YpSZ crystallizes into a mixture of cubic and tetragonal phases. The resulting XRD patterns were very sharp, which emphasizes the good crystallinity of the layer. Similar XRD results have already been discussed and reported in previous papers **[17, 18]**. FTIR spectra did not show any nitrate bands, thereby confirming a 100% conversion of nitrate precursors into oxide. The LPPR YpSZ coating appears to adhere well to the MCrAlY bond coat and perfectly fits the part shape. The arrow in Figure 9 shows an area where the LPPR YpSZ has infiltrated the MCrAlY bond coat.

Fig. 10 shows a cross-section microstructure of LPPR YpSZ deposited from 60 mL of diluted ($Std^{1/2}$) solution onto an alumina substrate. Similarly, as outlined above, the deposited LPPR YpSZ perfectly follows the alumina substrate roughness. Moreover, infiltration of YpSZ into the grain boundaries of the alumina substrate can be observed. This confirms that the selected deposition parameters enable the nitrate precursors to impact the surface in a liquid state, so that they can infiltrate and spread even between the alumina grains. This liquid diffusion creates

"anchorage points" that are favorable for the mechanical adhesion of the LPPR YpSZ coating to the substrate.

As a consequence, although a diluted solution results in an increased deposition time for a desired coating thickness, it has been chosen for the following repair tests. Indeed, a lower nitrate concentration reduces the risk of nitrate precursor precipitation and helps to maintain the precursors in a liquid state. This enables the nitrate precursors to properly infiltrate the areas of the damaged TBC to be repaired.

3.6 TBC local repair experiments without closing the cooling system on the combustor parts

Portions of a multi-hole combustion chamber (Hastelloy X/APS MCrAlY/ APS YpSZ) were cut out and artificially damaged with a micro tool machine, as described in Section 2.2. Fig. 11 shows two photographs of such combustor parts, before and after local repair by the scaled up LPPR. The deposition parameters were the same as those described in Section 3.5, using 400 mL of dilute ($Std^{1/2}$) solution for 10 hours of deposition. The protective gas flow was chosen as 2000 mL min^{-1} to fulfil the conditions of Section 2.3, corresponding to Eq. (3) and Eq. (4).

Indeed, considering the flow and density under STP conditions, Eq. (3) was verified as follows:

$F_{m\ holes} = 6 \times 10^{-5}$ kg s^{-1} < $F_{m\ prec} = 7.2 \times 10^{-5}$ kg s^{-1}.

Now, with regard to Equation 4: given that $\Sigma S_{poro} = 1.57 \times 10^{-5}$ m^2 (details of the calculation cannot be given) and considering the dimension of the plasma reactor, S_{reac} was calculated to be 7.85×10^{-3} m^2. As a result, Eq. (4) is: $F_{m\ holes} = 6 \times 10^{-5}$ kg s^{-1} ≥ $F_{m\ prec} \times (\Sigma S_{poro} / S_{reac}) = 1.44 \times 10^{-8}$ kg s^{-1}.

Finally, from Eq. (5), the Reynolds number was estimated at about 73 at the outlet of the holes, which is much less than 2100. All flux and dimension conditions required for the protection of cooling holes were validated for testing the repair.

After the repair experiment, the artificially damaged combustor part was actually coated with a new LPPR YpSZ layer and most of the cooling holes are visible and free of coating (Fig. 11). Cross-section SEM micrographs (Fig. 12) showed that the few plugged holes were either originally sealed (presence of APS TBC and MCrAlY bond coat inside) or obstructed by fine chips that were inserted when the artificial damage was inflicted. As is also reported in Fig. 12, the new deposited LPPR YpSZ did not clog the open holes. In any case, 100% of the holes

initially open remain free once the repair is completed. This validates the use of a protective gas, as long as its mass flow is well adjusted.

4. Conclusions

A low power plasma reactor was scaled up for local repair of thermal barrier coatings of real combustor parts. The reactor was equipped with an injector to introduce liquid nitrate precursor solutions into the low-pressure / low-power microwave plasma. A long spray distance associated with a high plasma power density lead to YpSZ coatings exhibiting a highly porous microstructure with large shell-like porosities. This microstructure is not suitable for ensuring both mechanical strength and adherence of the coating. A more interesting vertically cracked microstructure with reduced rounded porosities could be obtained with the following optimal parameters: high power plasma density of 7.35×10^{-4} W mm^{-3} (but with moderate plasma power of 1500 W), short spray distance of 240 mm and reduced precursor solution concentration. Furthermore, these parameters maintain the nitrate precursors in a liquid state during the flight time until they impact the substrate. As a consequence, the nitrates spread out and can efficiently infiltrate the substrate, which promotes the adherence of the YpSZ coating after conversion into

oxide through plasma post-treatment or later annealing. Such a LPPR is thus particularly suited for repairing TBC damage. Finally, it was demonstrated that a system involving two opposite gas flows allows the plugging of the cooling channels to be prevented during the local repair of a multi-hole combustion chamber, for example. Other important points under study are the determination of the mechanical strength, adhesion and high temperature durability of the LPPR YpSZ used for this local repair.

Acknowledgements

The authors would like to acknowledge the Agence Nationale de la Recherche and the Direction Générale de l'Armement for their financial support (N° ANR-13-ASTR-0017-02).

References

[1]: M.-P. Bacos, J.M. Dorvaux, O. Lavigne, R. Mévrel, M. Poulain, C. Rio, M.-H. Vidal-Sétif, *Performance and Degradation Mechanisms of Thermal Barrier Coatings for Turbine Blades: a Review of ONERA Activities,* Aerospace Lab, Issue 3 (2011).

[2]: P. Fauchais, *Understanding plasma spraying*, J. Phys. D: Appl. Phys., 33 (2004) pp R86-R108.

[3]: G. Mauer, R. Vaßen, D. Stöver, *Atmospheric plasma spraying of yttria-stabilized zirconia coatings with specific porosity*, Surf. Coat. Technol., 204 (2009), pp. 172-179.

[4]: U. Schulz, C. Leyens, K. Fritscher, M. Peters, B. Saruhan-Brings, O. Lavigne, J.M. Dorvaux, M. Poulain, R. Mévrel, M. Caliez, *Some recent trends in research and technology of advanced thermal barrier coatings*, Aerospace Sci. Technol., 3 (2003) pp. 73-80.

[5]: A. Biacciochini, F. Ben-Ettouil, E. Brousse, J. Ilavsky, G. Montavon, A. Denoirjean, S. Valette, P. Fauchais, *Quantification of void networks of as-sprayed and annealed nanostructured yttria-stabilized zirconia (YSZ) deposits manufactured by suspension plasma spraying*, Surf. Coat.Technol., Vol. 205, (2010), pp. 683-699.

[6]: A. G. Evans, D. R. Clarke, C.G. Levi, *The influence of oxides on the performance of advanced gas turbines*, J. of the Europ. Ceram. Soc., Vol. 28 (2008), pp. 1405-1419.

[7]: T. J. Radzavich, D. G. Nordstrom, K. D. Sheffler, *Method for preventing closure of cooling holes in hollow, air cooled turbine engine components during application of a plasma spray coating*, 1988, US Patent 4743462.

[8]: J. A Conner, *Method for preventing plating of material in surface openings of turbine airfoils*, 1997, US Patent 5985122.

[9]: D. Kang, K. Updegrove, F. Goodwater, *Plating turbine engine components*, 1998, US Patent 5800695.

[10]: G. F. Camm, *Method of unblocking an obstructed cooling passage*, 1999, US Patent 6004620.

[11]: Robert W. Bruce, *Method of removing a thermal barrier coating*, 2001, Brevet US 6210488.

[12]: W. R. Liebke, D. R. Dawson, M. A. Fredette, M. B. Goodstein, *Method of removing excess overlay coating from within cooling holes of aluminide coated gas turbine engine components*, 1997, US Patent 5702288.

[13]: J. A. Martus, P. P. Mehta, SeethaRamaiah Mannava, *Method for making or repairing a gas turbine engine component*, 1993, US Patent 5216808.

[14]: M-P. Bacos, O. Lavigne, C. Rio, M.-H. Vidal-Setif, F. Rousseau, D. Morvan, *Method for locally repairing thermal barriers*, 2017, October 11, European Patent EP3077570.

[15]: F. Rousseau, A. Quinsac, D. Morvan, M. P. Bacos, O. Lavigne, C. Rio, C. Guinard, B. Chevillard, *A new injection system for spraying nitrates in a Low Power Plasma Reactor : application to local repair of damaged Thermal Coatings*, Surf. Coat. Technol. 357, (2019), pp. 195-203.

[16]: C. Fourmond, G. Da Rold, F. Rousseau, C. Guyon, S. Cavadias, D. Morvan, R. Mevrel, *Characterization of thermal barrier coatings and ultra-high temperature composites deposited in a low pressure plasma reactor*, J. of the Europ. Ceram. Soc. 31, (2011), pp. 2295-2302.

[17]: F. Rousseau, C. Fourmond, F. Prima, M. H. Vidal Setif, O. Lavigne, D. Morvan, P. Chereau, *Deposition of thick and 50 % porous YpSZ layer by spraying nitrate solution in a low-pressure plasma reactor*, Surf. Coat. Technol. 206, (2011), pp. 1621-1627.

[18]: C. Fourmond, Synthèse d'oxydes par plasma, PhD Thesis, Pierre et Marie Curie University (Paris-France), 2011.

[19]: M-P. Bacos, F. Rousseau, D. Morvan, Procédé et système de dépôt d'oxyde sur composant poreux. 2016, August 16, European Patent EP3077569B1.

[20]: F. Rousseau, S. Awamat, D. Morvan, F. Prima, R. Mevrel, Yttria-Stabilized Zirconia thick coatings deposited from aqueous solution in a low-pressure plasma reactor, Surf. Coat. Technol. 203, (2008), pp. 442-448.

Parameters investigated	**Abbreviation**	**Values**	**Units**
Power	Pw	1200, 1700, 3000	W (Watt)
Power density	δ_p	3×10^{-4}, 4.2×10^{-4} and 7.35×10^{-4}	W mm^{-3}
Spray distance	d_{spray}	240, 500	mm
Standard solution concentration	Std	$[ZrO(NO_3)_2] = 3.4 \times 10^{-1}$ $[Y(NO_3)_3] = 2.96 \times 10^{-2}$	mol L^{-1}
Standard solution concentration diluted	$Std^{1/2}$	$[ZrO(NO_3)_2] = 1.7 \times 10^{-1}$ $[Y(NO_3)_3] = 1.48 \times 10^{-2}$	mol L^{-1}
Fixed LPPR parameters	**Nature**	**Values**	**Units**
Plasma gases	$Ar + O_2$	2000 + 500	ml min^{-1}
Gas for injector	Ar	2000	ml min^{-1}
Flow rate of solution	Std or $Std^{1/2}$	5	ml min^{-1}
Pulsed valve	opening time t_{on} / closing time t_{off}	0.8 / 1	s
Plasma pressure	-	700-1200	Pa

Table 1: summary of all the data explored or fixed for the deposition of YpSZ by LPPR

List of figure captions

Figure 1: Schematic view of the scaled-up Low Power Plasma Reactor (left) and of the deposition plasma chamber (right)

Figure 2: Local repair scheme for multi-hole components

Figure 3: Power density δ_p as a function of the applied plasma power for spray distances of 240 and 500 mm

Figure 4: FTIR spectra of LPPR YpSZ deposited at low and high power density values (spray distance: 500 mm)

Figure 5: Cross-section SEM micrographs (electron backscattered mode) of YpSZ coatings deposited at various plasma power and power density values (spray distance of 500 mm)

Fig. 6: SEM micrographs of a YpSZ coating surface (electron backscattered mode); deposition conditions: high power density of 7.35×10^{-4} W mm^{-3} corresponding to high power (3000W) and long spray distance (500 mm)

Figure 7: SEM micrographs (electron backscattered mode) of cross-sections of LPPR YpSZ coatings deposited with two different spray distances

Figure 8: Cross-section SEM micrograph (electron backscattered mode) of a YpSZ coating deposited onto a MCrAlY bond coat. Influence of the concentration of the nitrate solution on the deposited YpSZ microstructure

Figure 9: SEM cross-section micrograph (electron backscattered mode) of a YpSZ coating deposited from the diluted ($Std^{1/2}$) solution onto a MCrAlY bond coat

Figure 10: Cross-section SEM micrographs of a YpSZ coating deposited from the diluted (Std ½) solution onto an alumina substrate

Figure 11: Photograph of the same portion of combustor before (left) and after (right) TBC local repair using a scaled up LPPR : example of a hole observed by optical microscopy before and after the repair

Figure 12: Surface and cross-section SEM micrographs of a combustor portion before and after the repair: example of a hole closed by the original APS YpSZ and MCrAlY coatings and example of an open hole after deposition of LPPR YpSZ

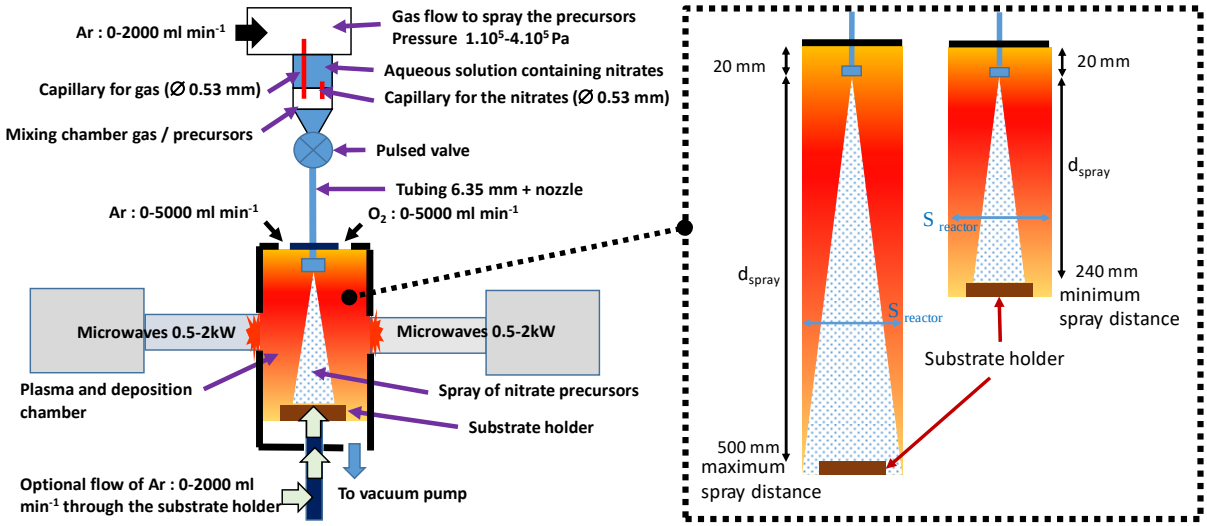
Ar : 0-2000 ml min-1
Gas flow to spray the precursors
Pressure 1.10^5-4.10^5 Pa
Aqueous solution containing nitrates
Capillary for gas (Ø 0.53 mm)
Capillary for the nitrates (Ø 0.53 mm)
Mixing chamber gas / precursors
Pulsed valve
Tubing 6.35 mm + nozzle
Ar : 0-5000 ml min-1
O2 : 0-5000 ml min-1
Microwaves 0.5-2kW
Microwaves 0.5-2kW
Plasma and deposition chamber
Spray of nitrate precursors
Substrate holder
Optional flow of Ar : 0-2000 ml min-1 through the substrate holder
To vacuum pump
20 mm
dspray
Sreactor
500 mm maximum spray distance
20 mm
dspray
Sreactor
240 mm minimum spray distance
Substrate holder

Figure 1

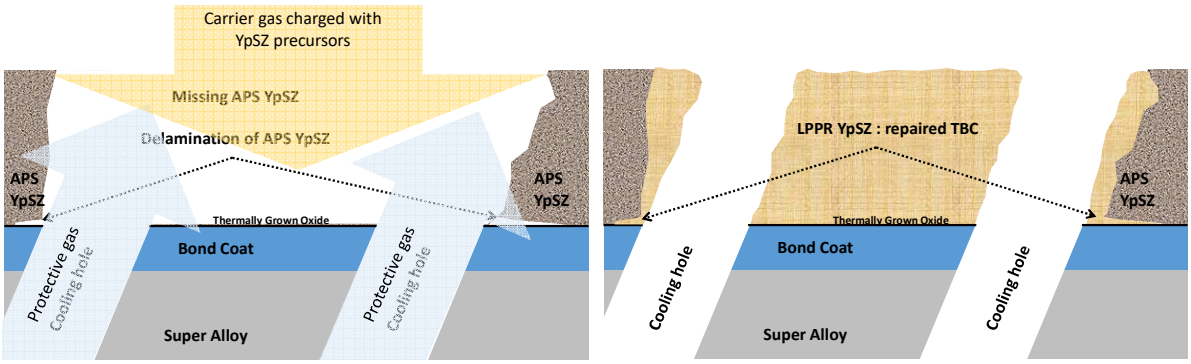
Carrier gas charged with
YpSZ precursors
Missing APS YpSZ
Delamination of APS YpSZ
APS
YpSZ
APS
YpSZ
Thermally Grown Oxide
Bond Coat
Protective gas
Cooling hole
Protective gas
Cooling hole
Super Alloy
LPPR YpSZ : repaired TBC
APS
YpSZ
Thermally Grown Oxide
Bond Coat
Cooling hole
Cooling hole
Super Alloy

Figure 2

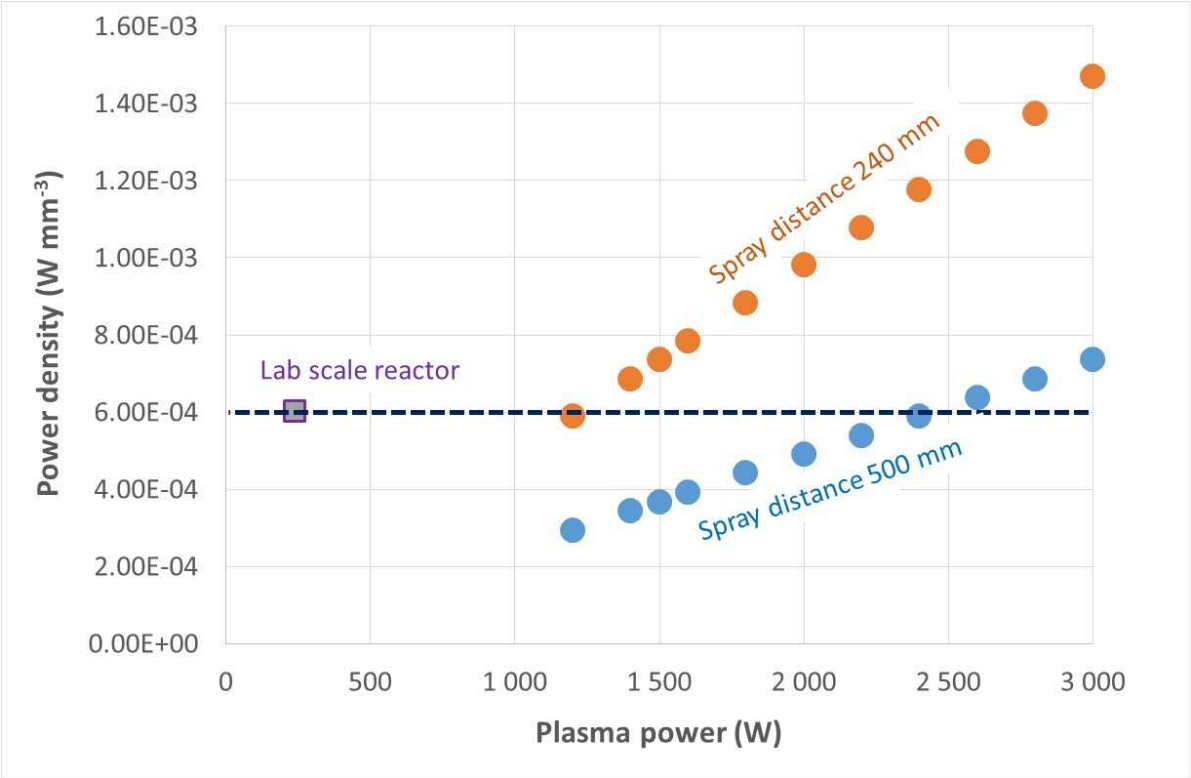
1.60E-03
1.40E-03
1.20E-03
1.00E-03
8.00E-04
6.00E-04
4.00E-04
2.00E-04
0.00E+00
Power density (W mm-3)
0
500
1 000
1 500
2 000
2 500
3 000
Plasma power (W)
Lab scale reactor
Spray distance 240 mm
Spray distance 500 mm

Figure 3

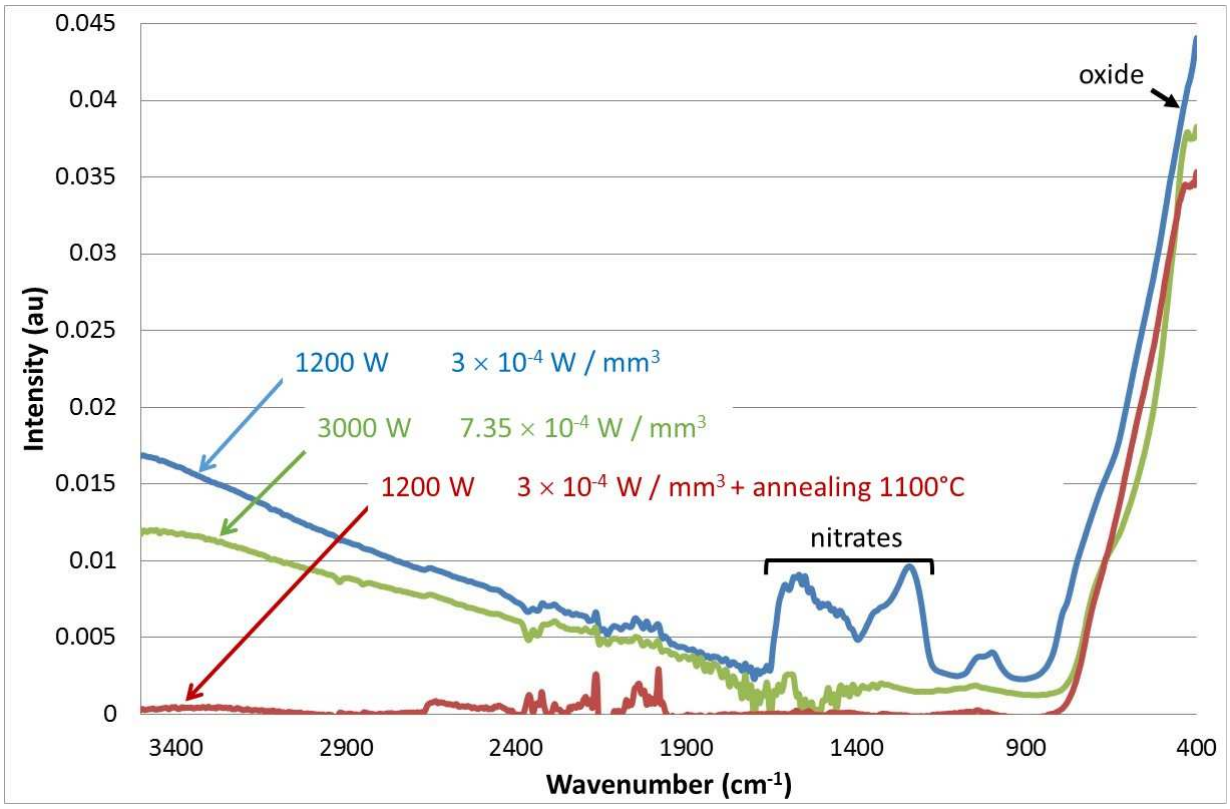
0.045
0.04
0.035
0.03
0.025
0.02
0.015
0.01
0.005
0
Intensity (au)
3400
2900
2400
1900
1400
900
400
Wavenumber (cm-1)
oxide
1200 W 3 × 10-4 W / mm3
3000 W 7.35 × 10-4 W / mm3
1200 W 3 × 10-4 W / mm3 + annealing 1100°C
nitrates

Figure 4

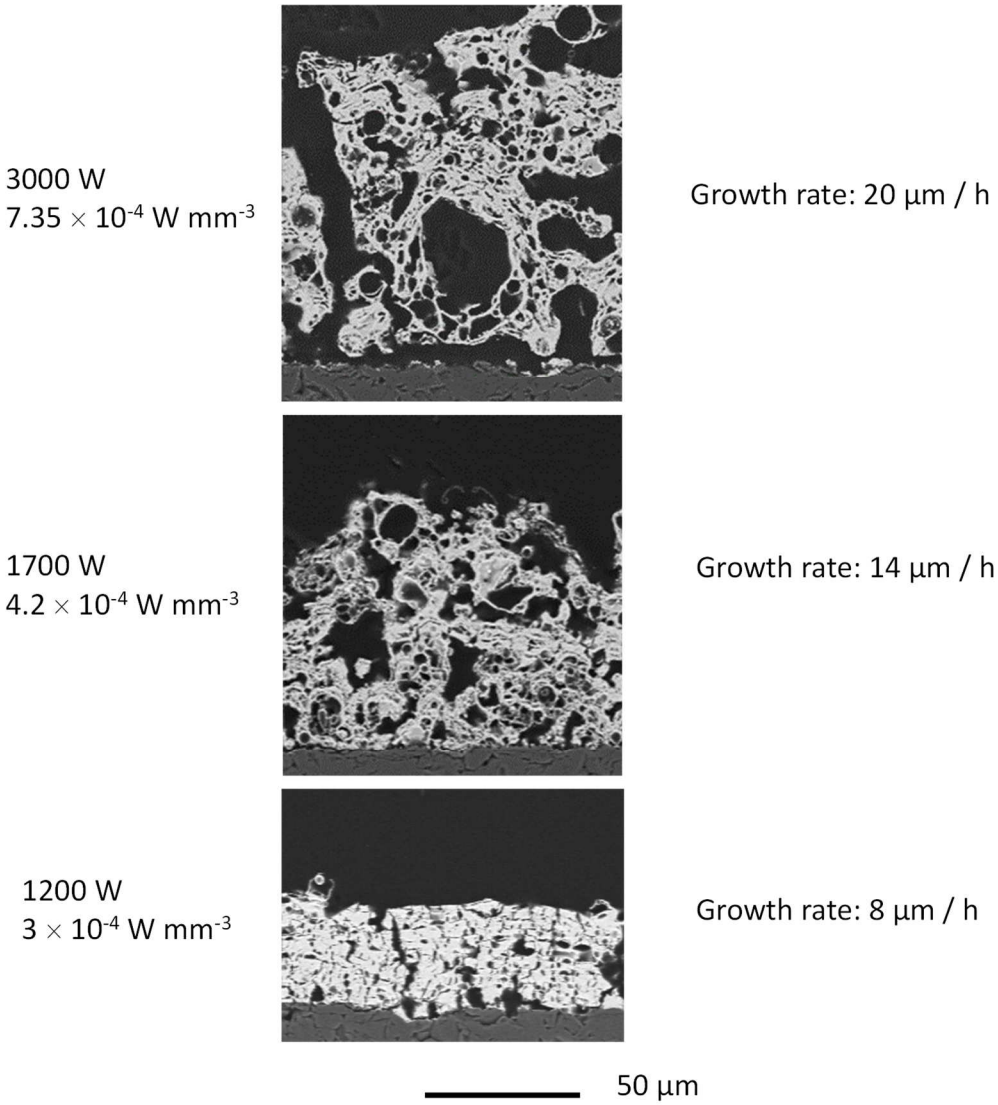
3000 W
7.35 × 10-4 W mm-3
Growth rate: 20 µm / h
1700 W
4.2 × 10-4 W mm-3
Growth rate: 14 µm / h
1200 W
3 × 10-4 W mm-3
Growth rate: 8 µm / h
50 µm

Figure 5

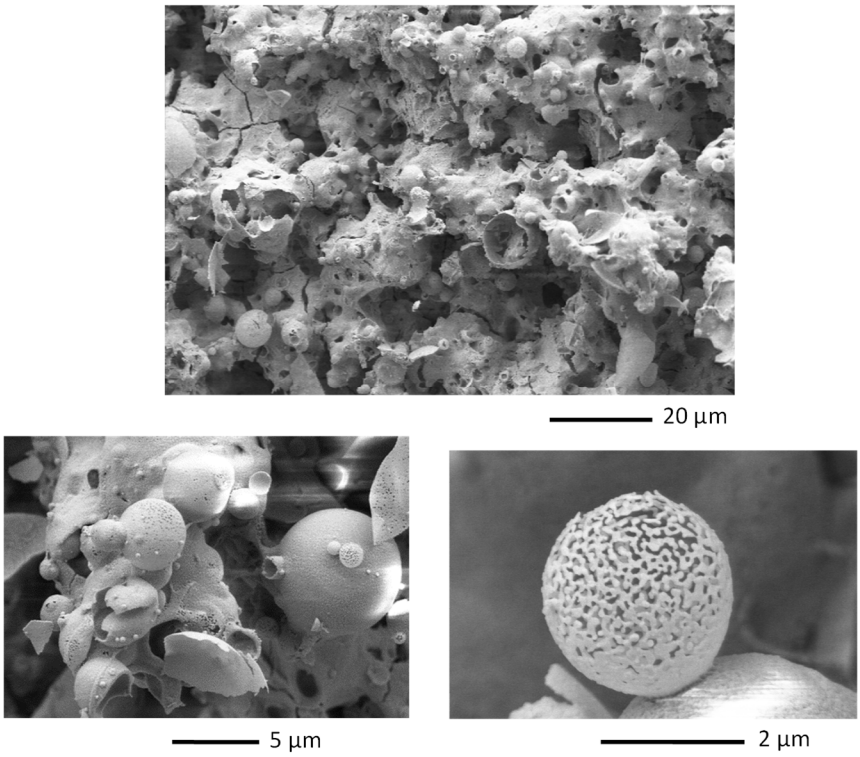

Figure 6

Spray distance 500 mm
3000 W
7.35×10^{-4} W mm^{-3}

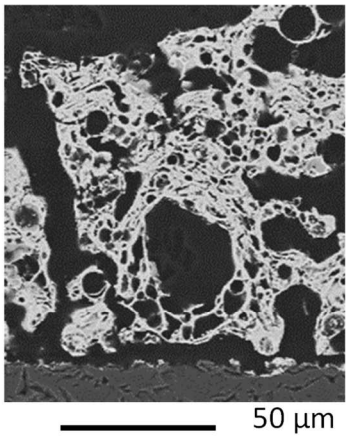

Growth rate: 20 µm / h

Spray distance 240 mm
1500 W
7.35×10^{-4} W mm^{-3}

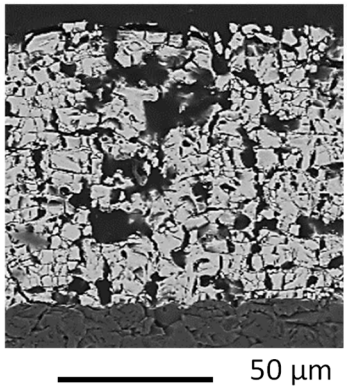

Growth rate: 20 µm / h

Figure 7

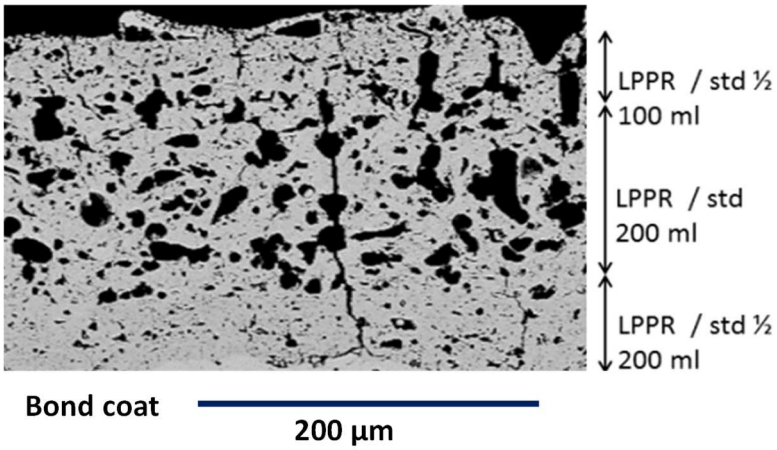
LPPR / std ½
100 ml
LPPR / std
200 ml
LPPR / std ½
200 ml
Bond coat
200 µm

Figure 8

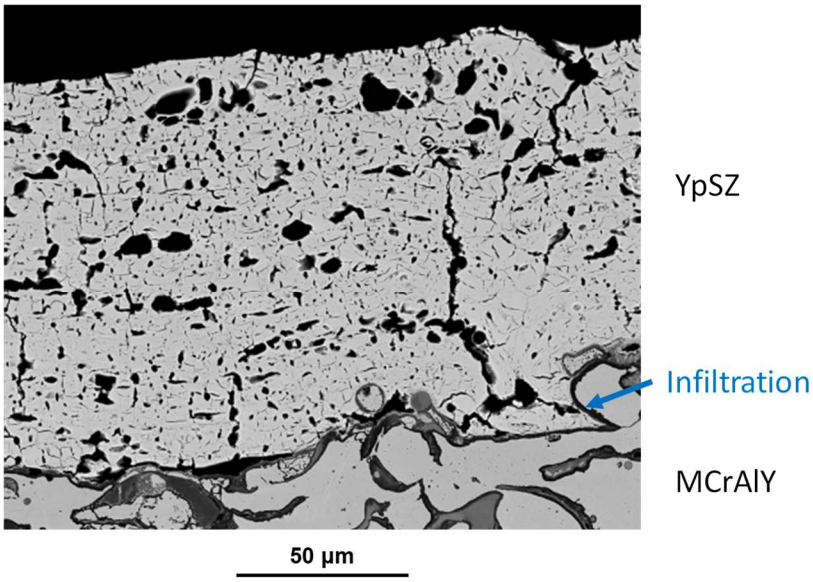

Figure 9

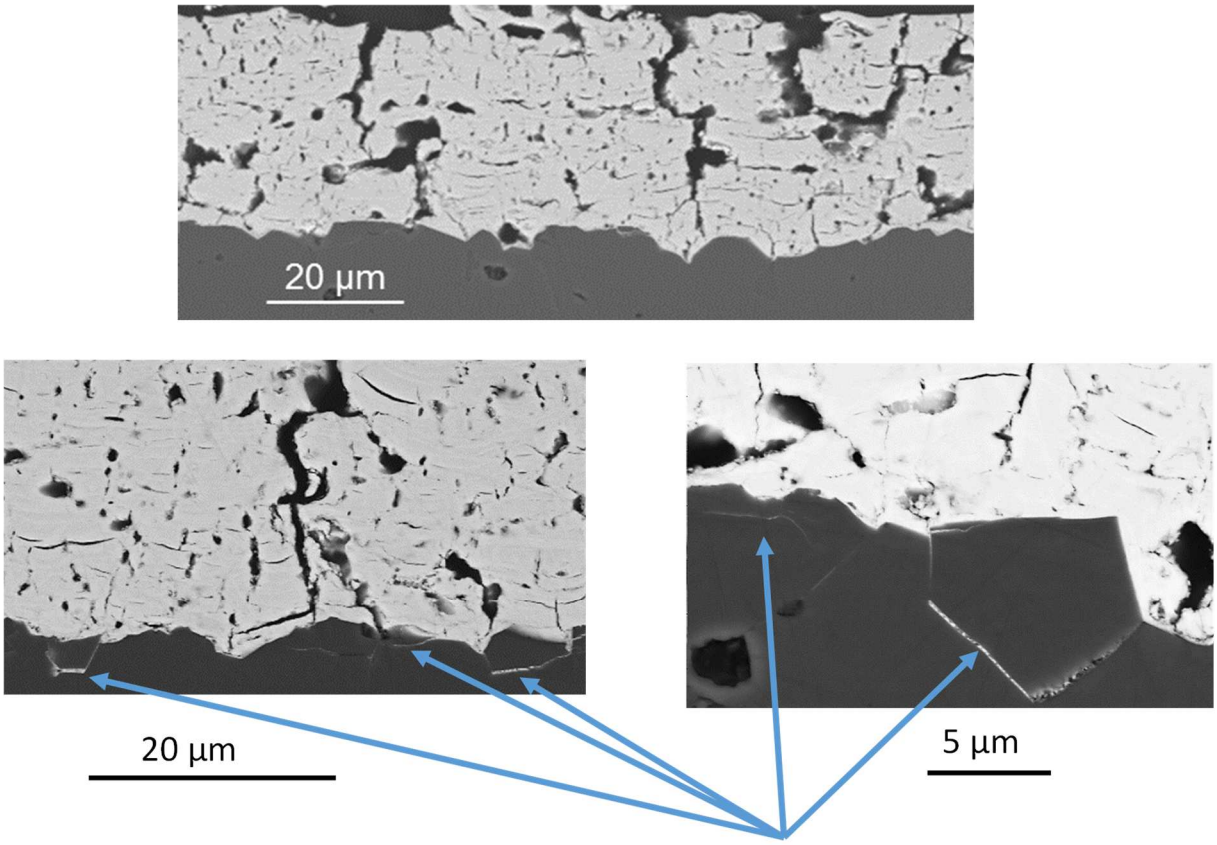
20 µm
20 µm
5 µm
Diffusion of liquid nitrates into grain boundaries to form YpSZ

Figure 10

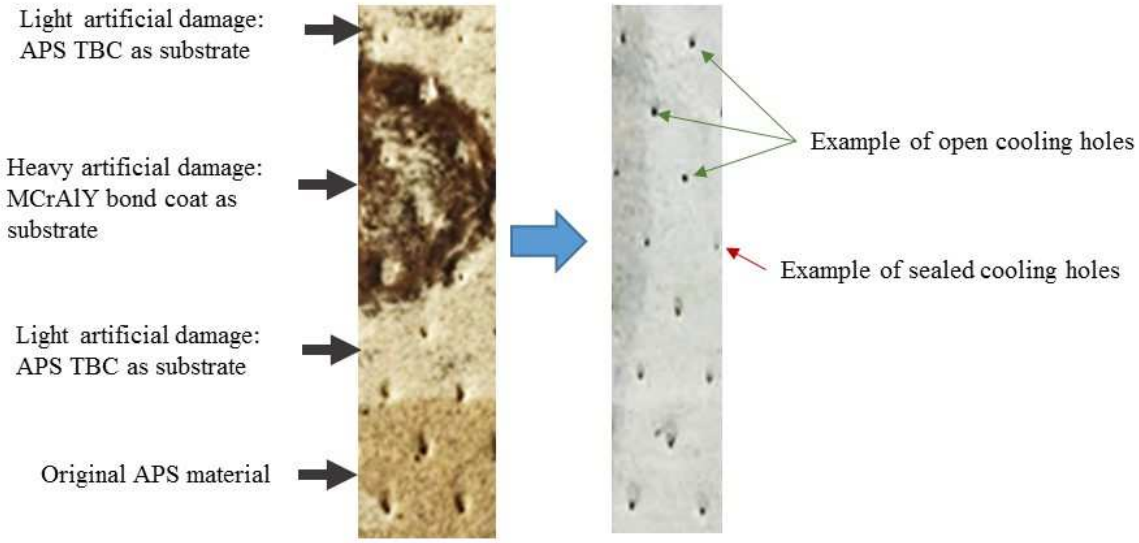

Same area observed before (left) and after the repair (right)

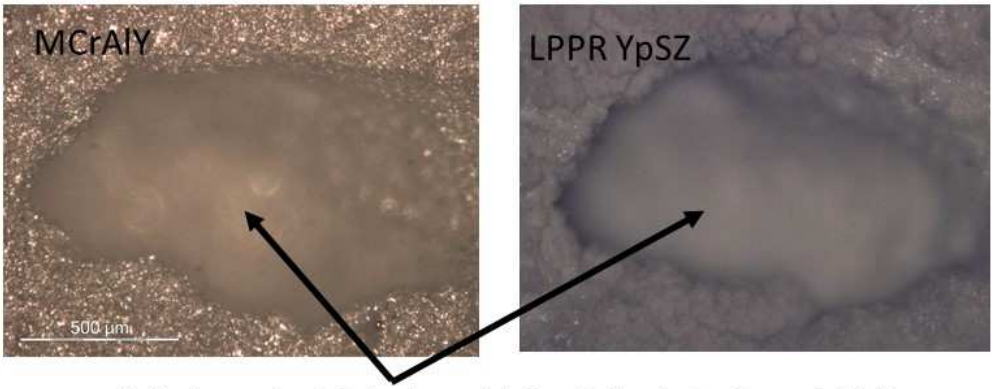

Optical micrograph of a hole observed before (left) and after the repair (right)

Figure 11

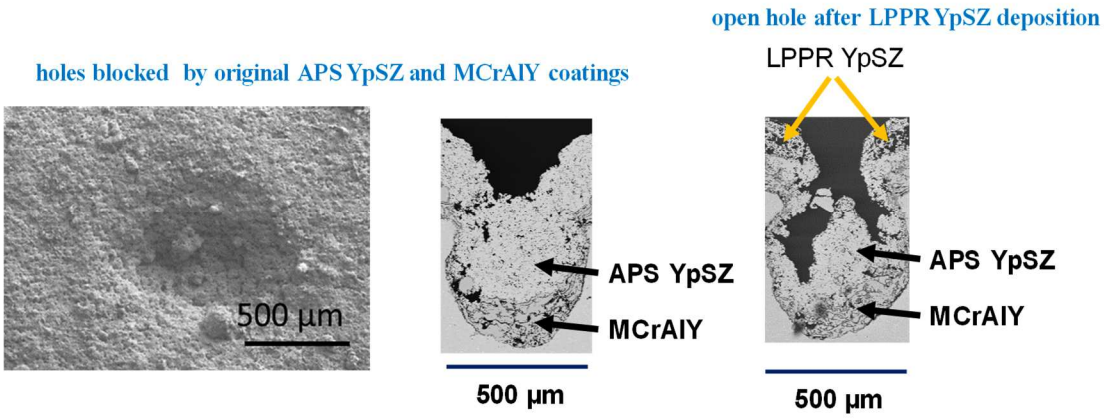
holes blocked by original APS YpSZ and MCrAlY coatings
500 µm
APS YpSZ
MCrAlY
500 µm
open hole after LPPR YpSZ deposition
LPPR YpSZ
APS YpSZ
MCrAlY
500 µm

Figure 12